Theses   Electronic Theses and Dissertations

11-2016

Fabrication and Characterization of Graphite Oxide Based Field Effect Transistors For Non Enzymatic Glucose-Sensor Application

Khadija Said Rahman

Follow this and additional works at: https://scholarworks.uaeu.ac.ae/all_theses

Part of the Physics Commons

UAEU

جامعة الإمارات العربية المتحدة
United Arab Emirates University

United Arab Emirates University

College of Science

Department of Physics

FABRICATION AND CHARACTERIZATION OF GRAPHITE OXIDE BASED FIELD EFFECT TRANSISTORS FOR NON-ENZYMATIC GLUCOSE-SENSOR APPLICATION

Khadija Said Rahman

This thesis is submitted in partial fulfilment of the requirements for the degree of Master of Science in Physics

Under the Supervision of Professor Naser Naim Qamhieh

November 2016

Declaration of Original Work

I, Khadija Said Rahman, the undersigned, a graduate student at the United Arab Emirates University (UAEU), and the author of this thesis entitled *"Fabrication and Characterization of Graphite Oxide Based Field Effect Transistors for Non-Enzymatic Glucose-Sensor Application"*, hereby, solemnly declare that this thesis is my own original research work that has been done and prepared by me under the supervision of Prof. Naser Naim Qamhieh, in the College of Science at UAEU. This work has not previously been presented or published, or formed the basis for the award of any academic degree, diploma or a similar title at this or any other university. Any materials borrowed from other sources (whether published or unpublished) and relied upon or included in my thesis have been properly cited and acknowledged in accordance with appropriate academic conventions. I further declare that there is no potential conflict of interest with respect to the research, data collection, authorship, presentation and/or publication of this thesis.

Student's Signature: _____   Date: __19 - 12 - 2016__

Advisory Committee

1) Advisor: Naser Naim Qamhich

Title: Professor

Department of Physics

College of Science, UAEU

2) Co-advisor: Ahmad Ayesh

Title: Associate Professor

Department of Mathematics, Statistics and Physics

College of Arts and Sciences, Qatar University

3) Member: Falah Awwad

Title: Associate Professor

Department of Electrical Engineering

College of Engineering, UAEU

Approval of the Master Thesis

This Master Thesis is approved by the following Examining Committee Members:

1) Advisor (Committee Chair): Naser Qamhieh

    Title: Professor

    Department of Physics

    College of Science, UAEU

    Signature _____ Date 3/11/2016

2) Co-advisor: Ahmad Ayesh

    Title: Associate Professor

    Department of Mathematics, Statistics and Physics

    College of Arts and Sciences, Qatar University

    Signature _____ Date 3/11/2016

3) Member: Falah Awwad

    Title: Associate Professor

    Department of Electrical Engineering

    College of Engineering, UAEU

    Signature _____ Date 3/11/2016

3) Member (External Examiner): Baker Mohammad

    Title: Associate Professor

    Department of Electrical Engineering

    Institution: Khalifa University, Abu Dhabi, UAE

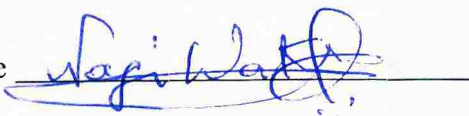   Signature _____ Date 3/11/2016

This Master Thesis is accepted by:

Dean of the College of Science: Professor Ahmed Murad

Signature _____   Date 19/12/2016

Dean of the College of the Graduate Studies: Professor Nagi T. Wakim

Signature _____   Date 20/12/2016

Copy 6 of 6

Abstract

Graphite-oxide based metal–oxide–semiconductor field-effect transistors (MOSFETs) were fabricated and used as glucose sensor. Herein, graphite-oxide was assembled between two planer electrical electrodes. The sensitivity of the sensor has been enhanced by adding copper (Cu) or silver (Ag) nanoparticles. The nanoparticles were produced by sputtering and inert gas condensation inside an ultra-high vacuum compatible system, and they were self-assembled on the graphite-oxide. The sensitivity of the sensor was increased by an order of magnitude when the silver nanoparticles were added. The sensitivity of each MOSFET was studied at different concentrations of non-enzymatic glucose for potential use in medical and industrial applications.

Keywords: MOSFET, Graphite Oxide, Graphene, Sensors, Non enzymatic glucose.

Title and Abstract (in Arabic)

تصنيع وتوصيف ترانزستورات تعتمد على أكسيد الجرافيت واستخدامها في استشعار الجلوكوز

الملخص

الهدف من هذه الااطروحة هو دراسة خواص ترانزستور (MOSFETs) المبني على معدن-أكسيد-شبه موصل-ترانزستور و دراسة حساسيته للجلوكوز. لقد تم تجميع أكسيد-الجرافيت بين أقطاب معدنية لدراسة الخواص الكهربائية. وقد تم تحسين حساسيته للكلوجوز بإضافة جزيئات النانو من النحاس (Cu) أوالفضة (Ag). هذه الجزيئات النانونية قد تم انتاجها بطريقة فيزيائية وذلك بانبعاث ذرات المعدن وتكثيفها باستخدام غاز خامل مثل الآرجون، وتجميعها على أكسيد-الجرافيت.

وأكدت الدراسة أن حساسية جهاز الاستشعار زادت عندما أضيفت جزيئات نانونية من الفضة في التراكيز العالية. وهذه الدراسة تشير لامكانية استخدام هذه الاداة في التطبيقات الطبية والصناعية.

مفاهيم البحث الرئيسية: MOSFET، أكسيد-الجرافيت، الجرافين، الحساسات، الجلوكوز غير الأنزيمي.

Acknowledgements

First and foremost, I praise God, the almighty for providing me this opportunity and granting me the capability to proceed successfully. I would like to thank all the people without whom this project would not be possible. Many people have contributed to this research in their own particular way and for that I am thankful.

I would like to express my special appreciation and thanks to my advisors Prof. Naser Naim Qamhieh, Physics Department, and Dr. Ahmad Ayesh, Department of Mathematics, Statistics and Physics, Qatar University. I would like to thank them for encouraging me during my research and for allowing me to grow as a research scientist.

Also, I greatly appreciate and thank. Prof. Saleh Thaker, Physics Department, Dr. Falah Awwad, Department of Electrical Engineering, who provided me with an excellent atmosphere for doing research.

My thanks extend to Dr. Soleiman Hisaindee, Department of Chemistry, for preparing graphite oxide solutions. Also, I want to thank Mr. Saeed Tariq, college of Medicine & Health Science, for his help to take the TEM images for the samples.

Special thanks go to my lovely parents, brothers, and sisters who helped me along the way. In addition, special thanks are extended to my mother, my sister Fatima, and brother Abdul Rehman for their assistance and encouragement.

Dedication

A special dedication to my lovely parents

To those who always give me love, support and encouragement
My brothers, sisters and friends

With their motivation, I accomplished this great achievement

Table of Contents

List of Figures

List of Abbreviations

Ag   Silver

Cu   Copper

EDS   Electron Dispersive Spectroscopy

GIC   Graphite Intercalation Compounds

GO   Graphite Oxide

MFC   Mass Flow Controller

MOSFETs   Metal–Oxide–Semiconductor Field-Effect Transistors

QCM   Quartz Crystal Monitor

QMF   Quadrupole Mass Filter

TEM   Transmission Electron Microscopes

UHV   Ultrahigh Vacuum

XRD   X-ray Diffractometer

Chapter 1: Introduction

1.1 Overview

Graphite consists of a multilayer hexagonally-structure, and carbon atoms in different layers are covalently bonded together. They are intercalated by various atoms and molecules due to the weak infrastructure of van der Waals forces. Graphite intercalation compounds (GIC) are prepared from different intercalation chemical species [1]. The partial oxidation of graphite becomes graphite-oxide (GO) [2-3]. The oxygen atoms are grouped on the edges of graphite and in the middle of the planes. GO contains carboxyl, phenolic hydroxyl and carbonyl groups that are founded by photoelectron spectroscopy [4-5]. Moreover, GO is characterized as solid layers [1], while graphene is a single layer of graphite [6]. GO has a high surface area [7], high charge carrier mobility at room temperature [8-9], low cost, and unique chemical, electronic, and nanostructure properties [10,11,12,13]. These properties make it attractive for fabricating various micro-electrical devices, for instance field effect transistors (FETs) [14], ultrasensitive sensors [11], electromechanical resonators [15], batteries [16] and biosensors [11]. Metal Oxide Field Effect Transistor (MOSFET) is an important type of transistors that is used for switching or amplification. MOSFET has three terminals: source, drain and gate. It can be either p-channel or n-channel, while the gate electrode is separated from the channel by an insulating oxide layer (SiO_2). The channel width, resistance and drain current (I_D) can be controlled by changing the gate to source voltage (V_{GS}) [17]. The advantage of using MOSFETs in variety of applications is due to that it is easy to vary V_{GS} at the gate and control the current flow in the channel [18].

Nowadays, the applications of glucose sensors vary because glucose participates on large scale in the process of human body metabolism [19]. Also, those sensors are important to measure glucose in the food industry and biological tissues [20].

On the other hand, diversity in nanoparticle sizes interferes in a variety of applications in the area of microelectronics [21,22]. Making the nanoparticles very small in size make the ratio of the surface to volume large, and the nanoparticles become more interactive with the surrounding environment of the system [23].

1.2 Aims and Objectives

In this work, different sizes of copper nanoclusters were prepared in ultrahigh vacuum compatible system (UHV). According to the optical, electrical, physical properties, the variation in the size of copper nanoparticles is important for sensors [24], optical devices [25] and catalytic implementations [21]. On the other hand, graphite-oxide (GO) based MOSFETs were fabricated, and used as non-enzymatic glucose sensors by utilizing the variation of GO resistivity when it is exposed to different concentrations of non-enzymatic glucose. Moreover, detecting low concentration from the non-enzymatic glucose solution is facilitated using graphite oxide devices decorated with (Cu or Ag) nanoparticles to enhance their sensitivity and response time [26]. Copper and silver are classified as good electrical conductors at low potential. In addition, the morphology, size, and (chemical/ physical) properties of metal nanoparticles play an important role in the interaction and absorption materials on the surface of nanoparticles [13,27], such as for glucose sensor applications.

1.3 Relevant Literature

Nanoparticles were successfully prepared physically by magnetron sputtering and inert gas condensation inside an ultra-high vacuum compatible system. Varying the fabrication conditions of the system allows producing different sizes of nanoclusters. This system is suitable for producing metallic nanoparticles like palladium (Pd) [28], silicon (Si), silver (Ag), etc. The sizes produced were in the order of few nanometers [29]. Moreover, by this system, nanoparticles composed of two different elements (bimetallic) were prepared [30].

Researchers utilized the variation in the conductivity property with the size of nanoclusters in many sensors applications. Zongxu Shen and his group, tested nonenzymatic glucose sensor based on the nickel nanoparticle–attapulgite-reduced graphene oxide-modified glassy carbon electrode (Ni-NPs/ATP/RGO). The lowest concentration they detected was 0.37 μM, and with linear range from 1 to 710 μM [31].

Also, nonenzymatic glucose sensor was detected by different nanoparticles such as copper (Cu) nanoparticles modified graphene sheets electrode [32], gold (Au) nanoparticles decorated on the reduced graphene oxide [33], palladium (Pd) nanoparticles functioned graphene (nafion–graphene) [34]. Furthermore, the reseachers also used the (PdCu) nanoparticles decorated three-dimensional graphene hydrogel (PdCu/GE) to detect the nonenzymatic glucose sensor, and the wide linear range they measured was from 1 mM to 18 mM [35]. Other reseach group used cobalt oxide nanoparticles (Co_3O_4-NPs) composite to detect an enzymatic glucose biosensor. A wide linear range they detected was from 0.5 mM to 16.5 mM [36]. Different type of nanoparticles (Mn_3O_4) decorated with nitrogen-doped reduced

graphene oxide (Mn$_3$O$_4$NP/N-rGO) has been used for sensing a non-enzymatic glucose [37]. A wider linear range (0.1 mM to 30.0 mM) was detected with a low detection limit of 0.02 mM by using PtAu–MnO2 binary nanocomposites decorated on the graphene paper [38].

Previous studies showed that researchers used the enzymatic biosensor to detect glucose because of their high sensitivity and selectivity. On the other hand, these sensors classified as week stability, and easily affected by the surrounding environment such as the humidity, temperature, and pH [39,40,41]. With the passage of time, non-enzymatic glucose became the substitutional to detect the glucose sensor [42-43]. Most of the nanoparticles were used to enhance the sensitivity of non-enzymatic glucose sensor suffered from low selectivity, low carriers mobility, and toxicity [39]. In the present work, a physical method is used to prepare the nanoparticles by using the UHV system, where it is easy to control and adjusted the size of the nanoparticles to suit variety applications such as detecting glucose sensor [29].

Chapter 2: Experimental

2.1 Device Fabrication

Figure 1 shows a schematic diagram for a MOSFET based on graphite-oxide that has been fabricated and used as a glucose sensor. The device was fabricated on top of a commercial heavily doped p type single face polished silicon wafer with 300 nm SiO_2 top layer. The wafers were sequentially cleaned via acetone, ethanol and deionized water, followed by a drying process using dried nitrogen gas. Electrical contact electrodes were deposited by standard thermal evaporation in a vacuum chamber of ~5 nm thick layer of NiCr and then on top of it ~50 nm layer of Au through a shadow mask [44]. The lower NiCr layer was used for better adhesion of the electrodes with the wafer [45]. The wafer was then diced into a proper size (1 cm × 0.5 cm), and cleaned again.
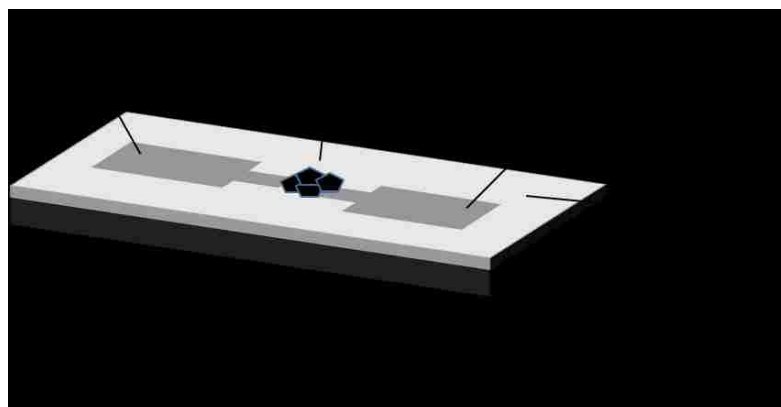

Figure 1: Schematic diagram of a graphite oxide based FET

2.2 Preparing Graphite Oxide Solution

Graphite oxide was synthesized from graphite using a modified Hummers method [46]. 5.00 g of graphite and 2.50 g $NaNO_3$ were mixed with 120 mL of

concentrated H_2SO_4 in a 500 mL flask. The mixture was stirred for 30 min in an ice bath, and 15.0 g potassium permanganate ($KMnO_4$) was added, in portions, to the suspension under vigorous stirring. The rate of addition was carefully controlled to keep the reaction temperature below 20 ℃. After addition was completed, the mixture was stirred twelve hours at room temperature and then 150 mL of H_2O was slowly added under vigorous stirring. The suspension was further stirred at 98 ℃ for 6 hrs. The mixture was cooled and 50 mL of 30% H_2O_2 was slowly added to destroy excess $KMnO_4$. The mixture was centrifuged, and the residue was washed several times with 5% HCl and then with deionized water. After filtration and drying under vacuum, 5.80 g of solid graphite oxide was obtained [47]. Finally 5mg/mL of graphite oxide was prepared by grinding 5 mg in 1 mL of distilled water and then exposed to the sonication for 45 minutes.

2.3 Testing the GO Device

A droplet of the solution was dropped between the gold electrodes on the SiO_2/Si substrate, and the device is left to dry for 24 hours at room temperature. The resistance of the device was measured during the deposition process of graphite-oxide solutions using an electrometer (Keithley 617) to confirm the establishment of percolation path(s). The doped Si substrate was used as a bottom gate of a field effect transistor. The current-voltage (I-V) measurements were used to characterize the device using a computer-controlled Keithley 236 source-measuring unit [48]. To prepare glucose solutions for testing the sensors, glucose powder was diluted in distilled water to form solutions with different concentrations of glucose, ranging from 1µM to 30mM. Moreover, different nanoparticles such as Ag and Cu were deposited on the surface of graphite-oxide to enhance their sensitivity [26].

2.4 Preparing Cu and Ag Nanoparticles

Copper and silver nanoparticles were fabricated using magnetron sputtering and inert gas condensation inside an ultrahigh vacuum compatible system (UHV) [29-30]. A schematic diagram for the nanoparticles generation source is shown in Figure 2. The base pressure in the system can reach 10^{-8} mbar by using a dry-rotary and two turbo pumps. Cu and Ag metals with a purity of 99.99% were used as targets, individually, and fixed on the sputter head. Where the sputter head and the source chamber were cooled by water under 15 C°. Argon gas with 99.999% purity was used to generate the plasma and also for nanoparticles condensation. The mass flow controller (MKS) instrument is used to control the inert gas flow rate (f_{Ar}) from range 0 to 100 ($\mp$ 0.5) sccm. This gas flow reaches the nanoclusters from the source chamber into the main chamber. It was found that the size of nanoparticles produced by this method is proportional to the fabrication parameters such as argon flow rate and sputtering discharge power [28]. For both Cu and Ag nanoparticles' production the argon gas flow rate used was 60 sccm. The discharge power used for sputtering to produce Cu and Ag nanoclusters were 97.47 W and 115.41 W, respectively. The distance between the target and the outlet nozzle of the source (aggregation length) was 40 mm. The aggregation length can be controlled by a motorized linear translator shown in Figure 2 without disturbing the vacuum of the source chamber. To control and analyze different nanocluster size distribution, a quadrupole mass filter (QMF) was used. The nanoclusters were produced in the source chamber, and then passing through the QMF to reach the main chamber. The QMF consists of four parallel metal rods that are connected electrically and opposite to each other. The potential applied between the rods is $+ (U + V \cos(\omega t))$ and $- (U + V \cos(\omega t))$, where

U is a DC voltage and V cos(ωt) is an AC voltage. The ratio U/V = 0.12 made the resolution clear and can be controlled by the mass scan. At the exit of the mass filter, a grid is located which works as Faraday cup. It measures the ion flux for certain selection of a nanoparticle's size, and the resulted current was measured by picoammeter [49]. In the main chamber, the nanoclusters were deposited on substrates, which are fixed on the sample holder that is facing the nanoclusters beam. The nanocluster deposition rate is measured by the quartz crystal monitor (QCM) which is fixed on a motorized linear translator that is moving forward in front of the nanocluster beam to measure the deposition rate, and moved backward far away from the beam.
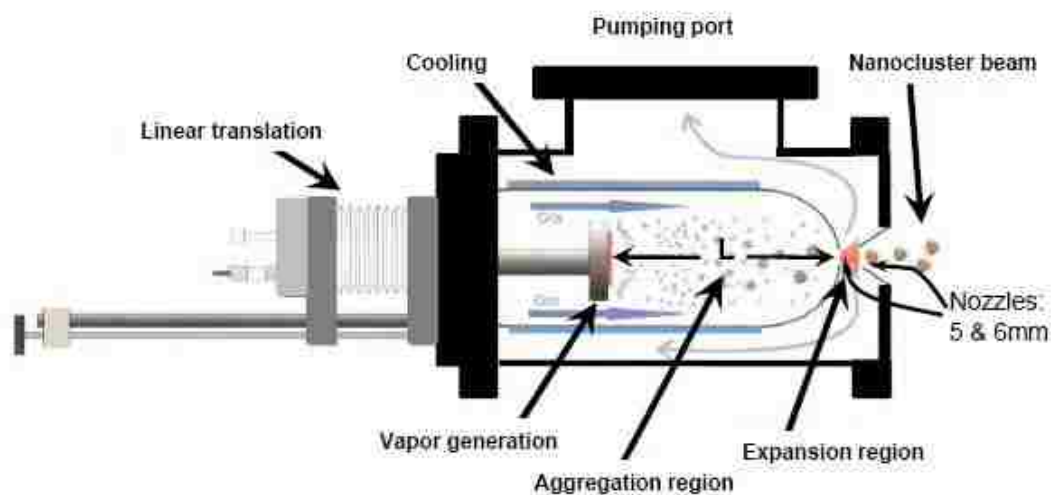

Figure 2: Schematic diagram of the cluster source [30]

2.5 Characterization of Cu and Ag Nanoparticles

Besides the graphite-oxide/Si/SiO$_2$ wafers, nanoparticles were deposited on glass and TEM grids to be used for nanoparticles' characterization. Herein, electron dispersive spectroscopy (EDS) was performed for elemental mapping analysis in

order to ensure the uniformity of the nanoparticles across the substrate. X-ray diffraction (XRD) using a Shimadzu 6100 X-ray diffractometer with Cu-Kα radiation ($\lambda = 1.5406$ Å) has been performed to study the structure and size of the nanoparticles. The presence and size of the nanoparticles has been confirmed using the Tecnai Biotwin Spirit G2 Transmission Electron Microscopes (TEM).

Chapter 3: Results and Discussion

3.1 Size Distribution of Nanoclusters

To demonstrate the fabrication process and the size selection of the nanoclusters, we present the data for producing Cu nanoclusters. The nanocluster size distribution measured by the QMF in the ultra-high vacuum system is shown in Figure 3. The nanocluster size distributions produced by varying aggregation length L starting from 40 and increased to 80 mm. It is clear in Figure 3 that the peak diameter D of the nanoclusters increases with increasing the aggregation length L at constant argon flow $f_{Ar} = 60$ sccm and the sputtering discharge power P = 73 W, with mass filter resolution U/V = 0.12. Moreover, the nanocluster diameter is D = 3.5 nm at low aggregation length L= 40mm, and current signal $I \approx 0.14 \, nA$. As the aggregation length increases, the diameter of nanoclusters increases and the current signal decreases. The peak diameter D in Figure 3 is plotted as a function of aggregation length L in Figure 4.

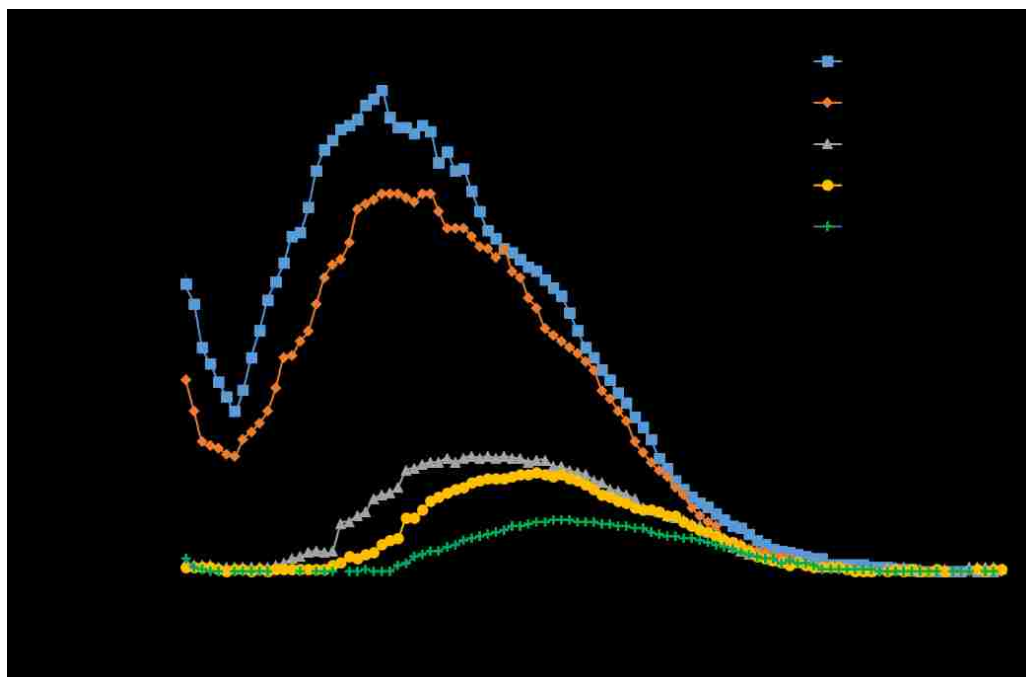Figure 3: Cu nanocluster size distributions produced for different aggregation length L, f_{Ar} = 60 sccm, U/V = 0.12 and P = 73 W

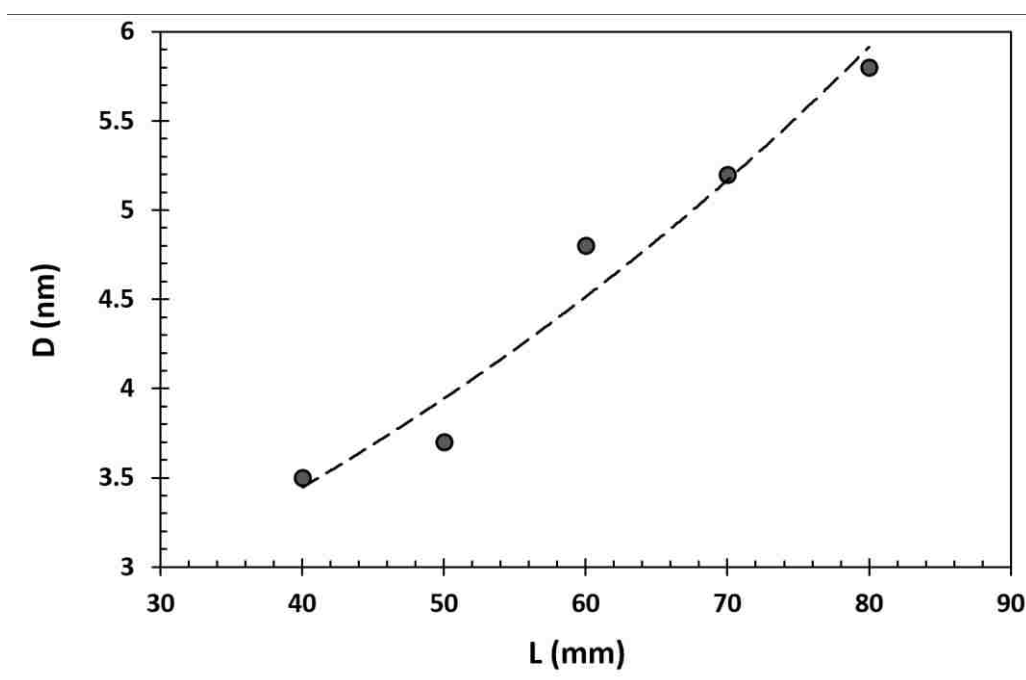Figure 4: The dependence of the peak diameter D on the aggregation length L at f_{Ar} = 60 sccm

Figure 4 shows that increasing the aggregation length L from L= 40 mm to L= 80 mm, leads to an increase in the peak diameter D. This result can be described in terms of the nucleation time. Where the nanoclusters remain long time before leaving the nanogenerator source for long aggregation lengths, and hence gives more chance to the nanoparticles size to build up [28].
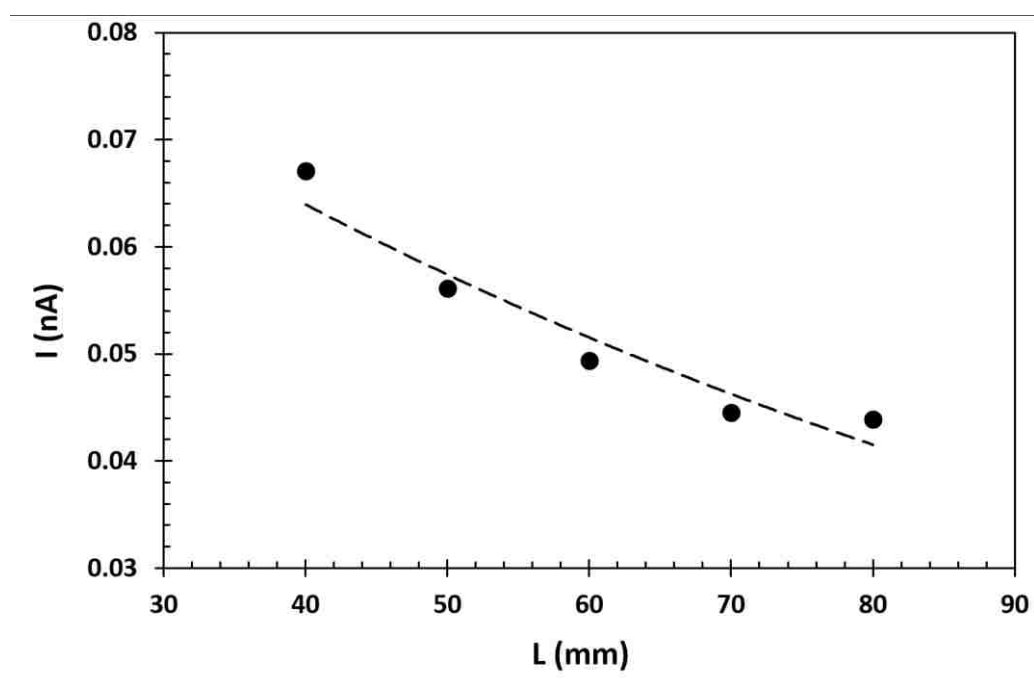
Figure 5: The dependence of the Cu nanocluster current signal of the peak diameter on L for f_{Ar} =60 sccm

Figure 5 shows the dependence of the nanocluster current signal at the peak of the size distributions on the aggregation length L presented in Figure 3. The current is related to the number of the charged nanoclusters crossing the area of the nozzle per unit time. According to Figure 4, the nanocluster size increases when the aggregation length increases. It can be explained in terms of two body collisions where nanocluster- nanocluster collisions are dominant to form bigger nanoclusters. This leads to a smaller number of big nanoclusters at long aggregation length L, as shown in Figure 5.

Figure 6: The dependence of the Cu nanoclusters yield on the aggregation length for P= 21.5W with different f_{Ar}

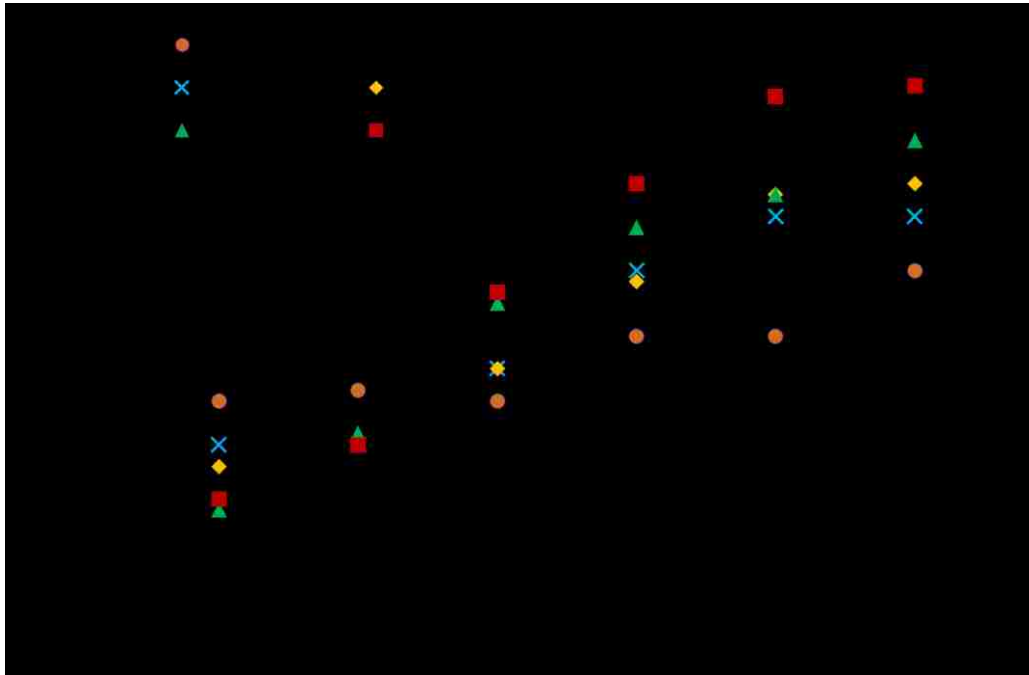Another parameter affects the size of the produced nanoclusters is the argon gas flow rate. Figure 6 shows the variation of the size with the aggregation length L at different Ar flow rate starting from f_{Ar} = 30 sccm to 80 sccm. The data shows that the peak diameter of the nanocluster increases with the increase in L by 1.5 nm at low Ar flow, where the slope of the curve $\Delta D/\Delta L$ is small. On the other hand at high Ar flow rate the slope $\Delta D/\Delta L$ of the variation of D with L is bigger. The graph shows higher value for the slope increases by 4 nm at high Ar flow rate. Increasing the argon flow rate sweeps the nanoclusters very quickly out the generation source leaving more room for nanocluster seeds nucleation [29].

3.2 Characterizing the Nanoparticles

Figure 7 shows the transmission electron microscope (TEM) image and size distribution of silver nanoparticles. TEM image appears clearly the relatively

spherical shape of silver nanoparticles (Ag-NPs). The average diameter of Ag-NPs is around 7 nm, and the size distribution is in the diameter range of 2 nm to 7 nm as shown in Figure 7 (b). While the TEM image and the size distribution of Cu-NPs produced is shown in Figure 7. Also the relatively spherical shape appears for Cu-NPs as shown in TEM image Figure 8(a). From Figure 8(b), the average diameter of Cu-NPs is around 6 nm and mostly the large size covered for copper nanoparticles are ranged from 5 nm to 9 nm.
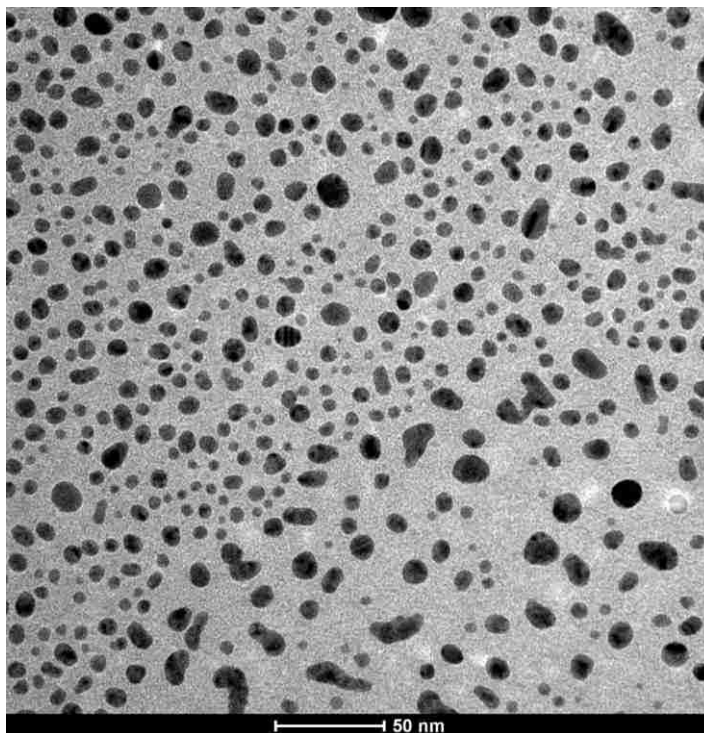
(a)
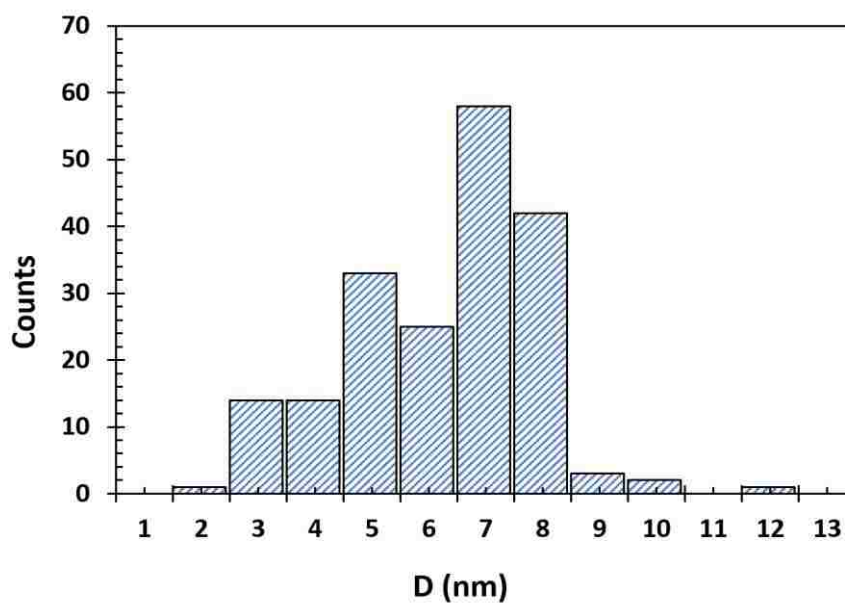
(b)

Figure 7: (a) TEM image of Ag nanoparticles. (b) Size distribution of Ag nanoparticles

(a)
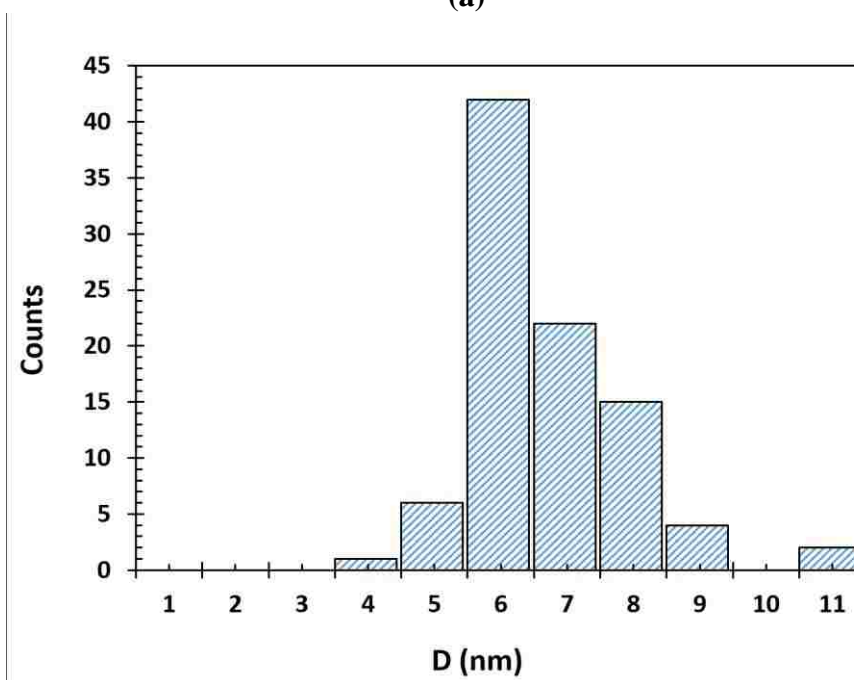
(b)

Figure 8: (a) TEM image of Cu nanoparticles. (b) Size distribution of Cu nanoparticles

The energy dispersive spectroscopy confirmed the elemental existence for both silver and copper nanoparticles as illustrated in Figures 9(a) and 10(a), respectively. It is shown that the amount of mass percentage for silv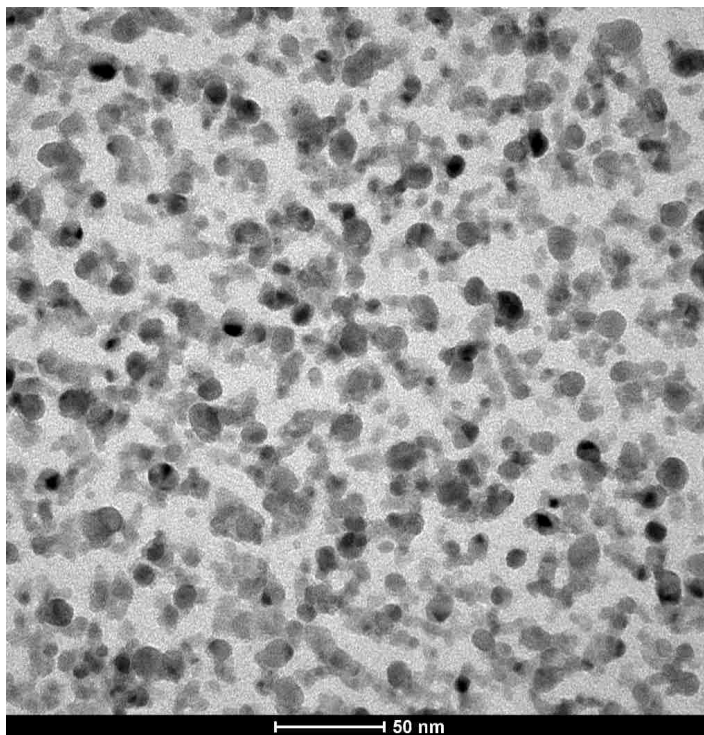er nanoparticles, about 0.75 Wt. %, while for copper nanoparticles the mass percentage is about 2.62 Wt. %. Silicon, carbon, oxygen are appeared in the EDS spectrum due to oxidation of the nanoparticles and the emission from the elements of the glass substrate used for the EDS analysis.

XRD measurements analysis the composition of the produced Ag and Cu nanoparticles as illustrated in both Figures 9(b) and 10(b), respectively. The peaks at angles of 2θ equal 38, 44, 64, and 77 correspond to Bragg reflection from face centered cubic (fcc) planes at (111), (200), (220), and (311) planes related to the Ag-NPs as shown in Figure 9(b), which agree with results in reference [50]. While the corresponding angles for Cu-NPs at 2θ at 44, 64, and 77 represent the peaks from face centered cubic planes (111), (200), and (220) as shown in Figure 10(b), and it is well agree with the data in reference [51].
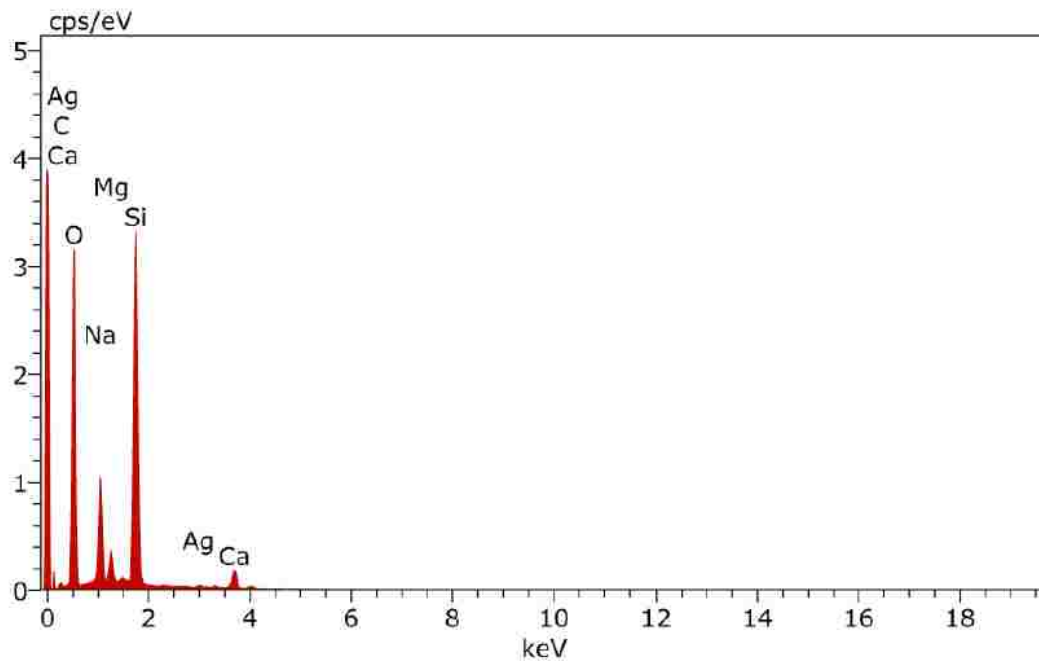
Spectrum: Ag.spx

El	AN	Series	unn. C [wt.%]	norm. C [wt.%]	Atom. C [at.%]	Error (1 Sigma) [wt.%]
C	6	K-series	5.10	3.26	5.08	1.48
O	8	K-series	90.59	58.00	67.73	11.06
Na	11	K-series	18.91	12.11	9.84	1.28
Mg	12	K-series	5.15	3.30	2.53	0.33
Si	14	K-series	32.08	20.54	13.66	1.41
Ca	20	K-series	3.61	2.31	1.08	0.15
Ag	47	L-series	0.75	0.48	0.08	0.07
		Total:	156.19	100.00	100.00	

(a)
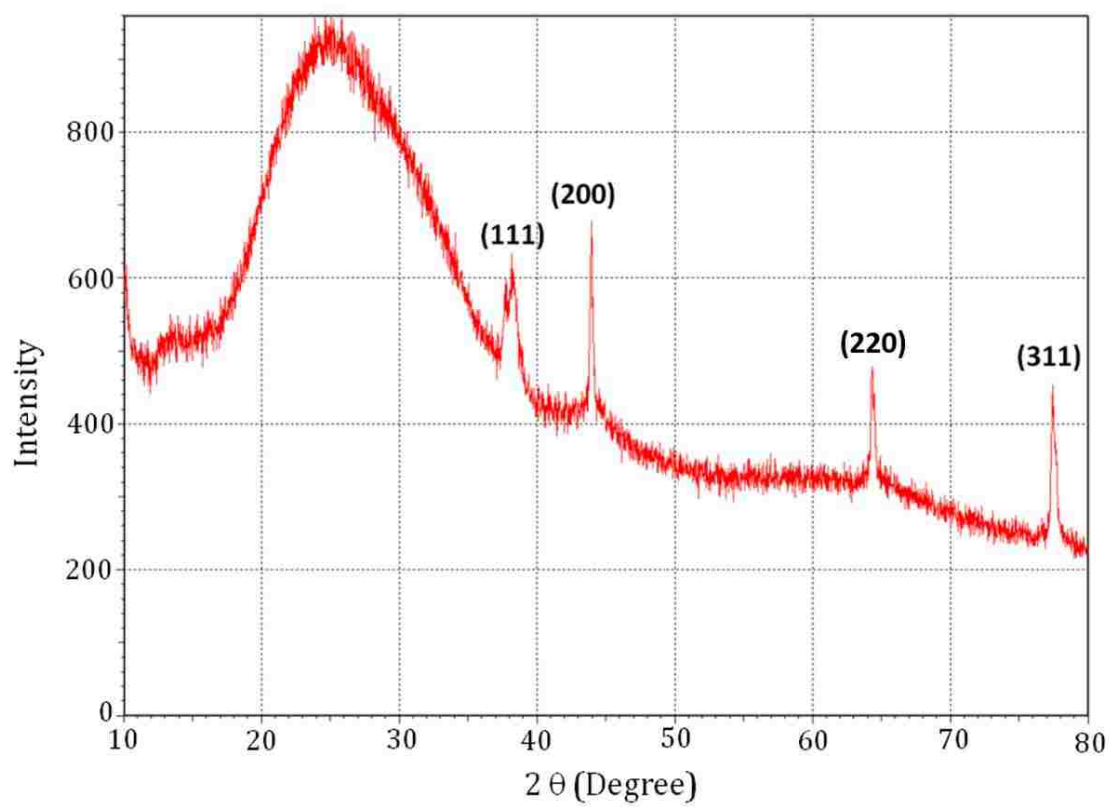
(b)

Figure 9: (a) EDS and (b) XRD spectra of the produced Ag nanoparticles
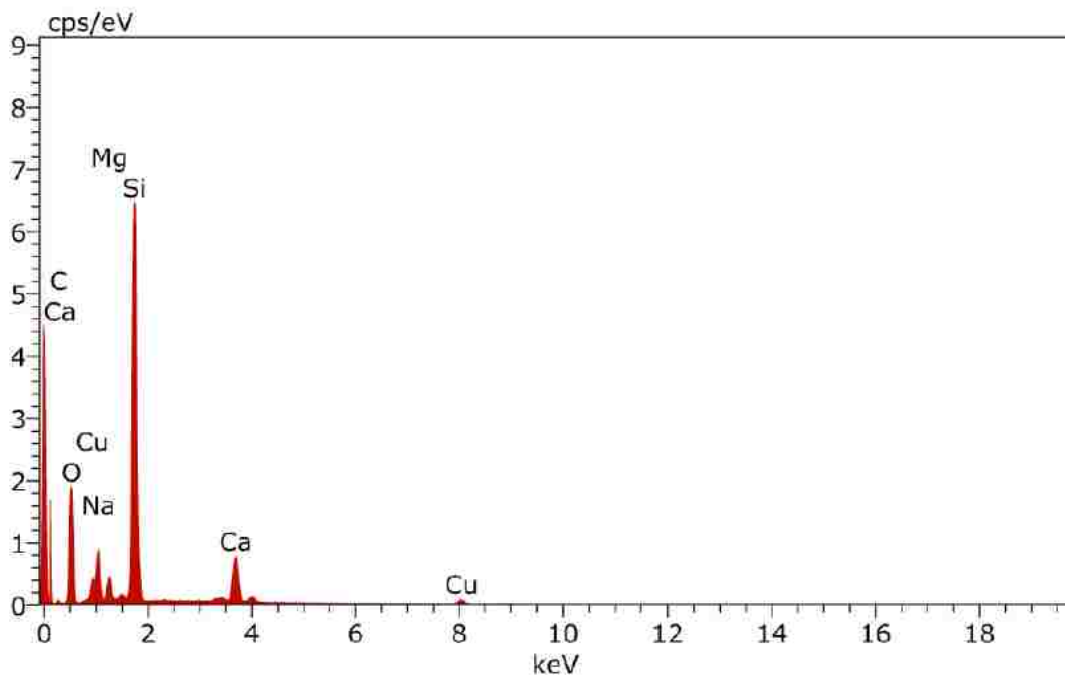
Spectrum: CU.spx

El	AN	Series	unn. C [wt.%]	norm. C [wt.%]	Atom. C [at.%]	Error (1 Sigma) [wt.%]
C	6	K-series	2.85	3.55	6.14	0.76
O	8	K-series	34.79	43.32	56.26	4.36
Na	11	K-series	6.14	7.64	6.91	0.43
Mg	12	K-series	2.03	2.53	2.17	0.14
Si	14	K-series	24.99	31.12	23.02	1.09
Ca	20	K-series	6.88	8.57	4.44	0.23
Cu	29	K-series	2.62	3.26	1.07	0.12
		Total:	80.31	100.00	100.00	

(a)
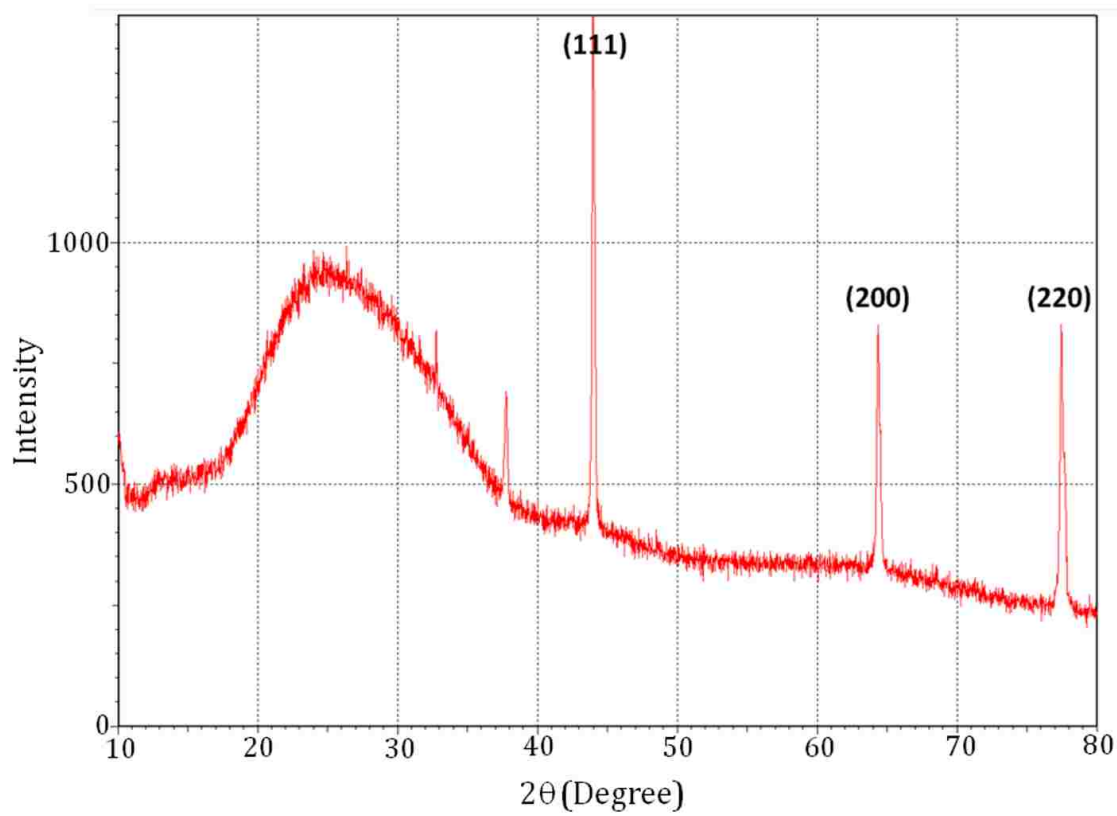
(b)

Figure 10: (a) EDS and (b) XRD spectra of the produced Cu nanoparticles

XRD measurements can be used to calculate the average nanoparticle size (D) using

Scherrer's equation:

$$D = \frac{k\lambda}{\beta cos\theta} \qquad (1)$$

Where k is a dimensionless constant related to the shape of nanoparticles, and it is taken 0.94 in the present calculations. λ is the wavelength of X-ray, β is the full width at half maximum of an X-ray peak, and θ is the Bragg's angle.

Realizing the average spherical size of nanoparticles is performed using Scherrer's equation at diffraction peaks (200) and (111) for Ag-NPs and Cu-NPs, respectively, that have the highest intensities. The average size is equal to 14.2 nm for Ag-NPs, while it is 15.7 nm for Cu-NPs. The overestimation of nanoparticle size compared with the results obtained from the TEM images can be assigned to the agglomeration of nanoparticles in the samples prepared for the XRD measurements, where sample thickness is ~100 nm.

3.3 FET Characteristics

Figure 11 shows I_D-V_{DS} characteristics at different gate voltages for a graphite oxide MOSFET. The drain source voltage varies from V_{DS} = -40 to 40 V, and the measurements were performed at room temperature. The curves are nonlinear and I_D increases with increasing V_{DS} for each value of V_{GS}. Moreover, the n-type nature of charge carriers in the conducting channel between the drain and the source explains the effect of varying V_{GS} on the I_D-V_{GS} curves. Decreasing the value of V_{GS} leads to a reduction in the density of conducting charge carriers (electrons) in the channel, and consequently to a decrease in the drain current I_D. Eventually, when the value of V_{GS} becomes negative electrons are depleted from the channel leading to

a reduction in the channel conductivity. The positive gate voltage abundances the density of conducting electrons in the channel and enhances the channel conductivity, and consequently the drain current I_D.
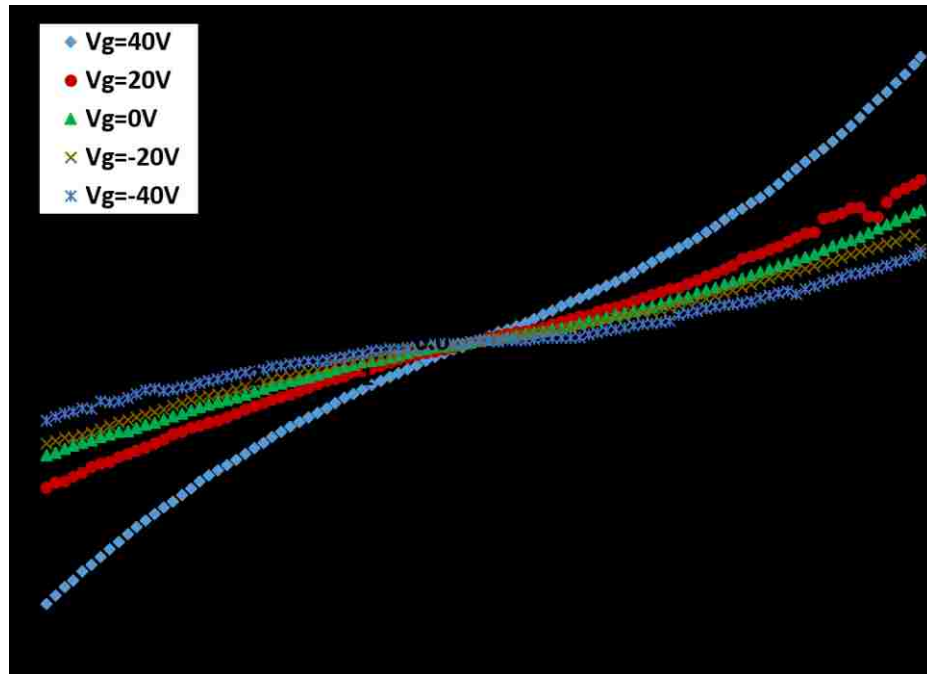
Figure 11: I_D-V_{DS} characteristics for the graphite oxide gate measurements

3.4 Sensor Testing

The sensitivity of graphite oxide to non-enzymatic glucose is tested by measuring the current I_D (at a constant V_{DS}) and monitors the change in its value when exposed to glucose. A typical measurement is shown in Figure 12 with a gate voltage $V_{GS} = 0$ V and $V_{DS} = 0.1$ V, the current started at $I_{max} = 3.01 \times 10^{-5} \mp 0.189$ A. When the graphite oxide is exposed to 30 mM non-enzymatic glucose solution at time t = 4s, a sharp drop in the current is observed and reach a value about $I_{min} = 0.32 \times 10^{-5} \mp 0.185$ A, and then it becomes nearly constant. Calculating the change in the current is used to measure the sensitivity of the graphite oxide sensor to glucose using:

$$\Delta I = I_{max} - I_{min} \qquad\qquad (3)$$
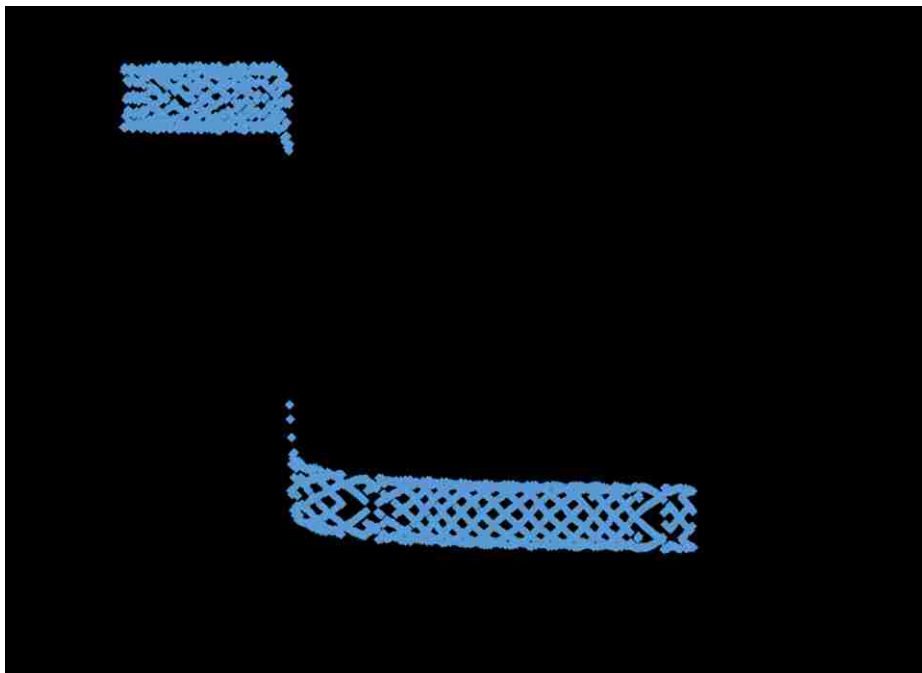
Figure 12: Change in the current (Δ I) at 30 mM non-enzymatic glucose

The test was repeated for different concentrations of glucose, from 1μM to 30 mM, in the solution and the data is plotted in Figure 12. The curve shows that the sensitivity (ΔI) of the sensor increases with increasing the glucose concentration with an abrupt increase at about 1μM glucose concentration. The comparative sensitivity between GO and GO/Cu-NPs shows that the sensitivity increases by adding Cu nanoparticles on GO. Also Figure 12 includes measurements of the sensitivity using Ag nanoparticles. Adding Ag-NPs on the top of GO increases the sensitivity of the sensor sharply as shown in the figure. According to the TEM images, the average size of Ag nanoparticles is larger than that of Cu nanoparticles that tend to be small size particles [52]. The figure shows that sensors based on GO with Cu-NPs are more suitable for detecting low concentrations of glucose. Cu nanoparticles can be easily a container to the functional group of oxygen in GO [53]. Also, the spherical shape of

Cu nanoparticles provide active sites for the oxidation of glucose and large specific surface area for further reactive sites. Moreover, low cost, wide range detection, higher sensitivity, high electrochemical reactions, fast electron transfer at low potential, and easy chemical with physical interaction with the glucose solution [26], lead to choose GO/Cu-NPs to enhance the sensitivity of non-enzymatic glucose sensor at low concentrations of glucose more than GO/Ag-NPs. Where, Ag nanoparticles were classified as weak to detect low concentration of glucose [53].
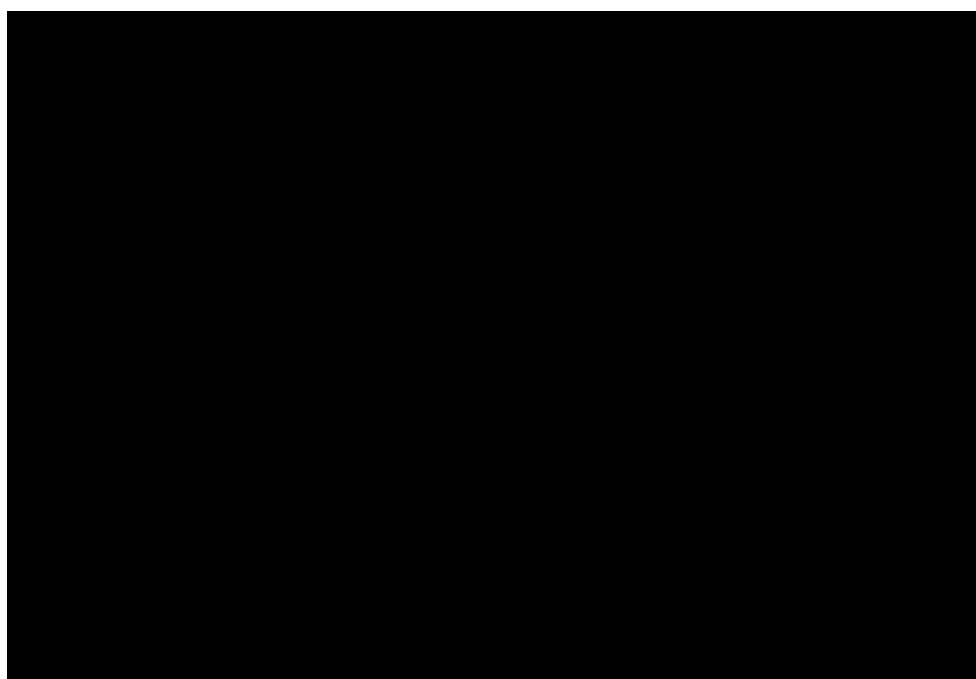
Figure 13: Change in the current (Δ I) at different concentrations of non-enzymatic glucose solution for GO, GO/CuNPs, and GO/AgNPs

Chapter 4: Conclusions

Graphite oxide based metal–oxide–semiconductor field-effect transistors (MOSFETs) were fabricated, tested and enhanced by introducing Cu and Ag nanoparticles at their surface. The graphite-oxide MOSFETs were used to sense a concentration as low as of glucose solution. Adding Cu or Ag nanoparticles (NPs) have enhanced the sensor's sensitivity. The advantages of using GO/Cu-NPs and GO/Ag-NPs are good reproducibility, stability, instantaneous with low detection sensitivity at about 1 μM, and the wide range detection from 1μM up to 30 mM.

References

[1] Ramesh, P., Bhagyalakshmi, S., & Sampath, S. (2004). Preparation and physicochemical and electrochemical characterization of exfoliated graphite oxide. Journal of colloid and interface science, 274(1), 95-102.

[2] Hirata, M., Gotou, T., Horiuchi, S., Fujiwara, M., & Ohba, M. (2004). Thin-film particles of graphite oxide 1:: High-yield synthesis and flexibility of the particles. Carbon, 42(14), 2929-2937.

[3] Yang, C., Wu, S., Cheng, J., & Chen, Y. (2016). Indium-based metal-organic framework/graphite oxide composite as an efficient adsorbent in the adsorption of rhodamine B from aqueous solution. Journal of Alloys and Compounds, 687, 804-812.

[4] Peckett, J. W., Trens, P., Gougeon, R. D., Pöppl, A., Harris, R. K., & Hudson, M. J. (2000). Electrochemically oxidised graphite.: Characterisation and some ion exchange properties. Carbon, 38(3), 345-353.

[5] Talyzin, A. V., Solozhenko, V. L., Kurakevych, O. O., Szabó, T., Dékány, I., Kurnosov, A., & Dmitriev, V. (2008). Colossal Pressure-Induced Lattice Expansion of Graphite Oxide in the Presence of Water. Angewandte Chemie International Edition, 47(43), 8268-8271.

[6] Schniepp, H. C., Li, J. L., McAllister, M. J., Sai, H., Herrera-Alonso, M., Adamson, D. H., ... & Aksay, I. A. (2006). Functionalized single graphene sheets derived from splitting graphite oxide. The Journal of Physical Chemistry B, 110(17), 8535-8539.

[7] Oshima, C., & Nagashima, A. (1997). Ultra-thin epitaxial films of graphite and hexagonal boron nitride on solid surfaces. Journal of Physics: Condensed Matter, 9(1), 1.

[8] Basiruddin, S. K., & Swain, S. K. (2016). Phenylboronic acid functionalized reduced graphene oxide based fluorescence nano sensor for glucose sensing. Materials Science and Engineering: C, 58, 103-109.

[9] Chen, J. H., Jang, C., Xiao, S., Ishigami, M., & Fuhrer, M. S. (2008). Intrinsic and extrinsic performance limits of graphene devices on SiO2. Nature nanotechnology, 3(4), 206-209.

[10] Novoselov, K.S., Geim, A.K., Morozov, S.V., Jiang, D., Zhang, Y., Dubonos, S.V., Grigorieva, I.V. and Firsov, A.A. (2004). Electric field effect in atomically thin carbon films. science, 306(5696), 666-669.

[11] Schedin, F., Geim, A. K., Morozov, S. V., Hill, E. W., Blake, P., Katsnelson, M. I., & Novoselov, K. S. (2007). Detection of individual gas molecules adsorbed on graphene. Nature materials, 6(9), 652-655.

[12] Pumera, M. (2011). Graphene in biosensing. Materials Today, 14(7), 308-315.

[13] Dhara, K., Ramachandran, T., Nair, B. G., & Babu, T. S. (2015). Single step synthesis of Au–CuO nanoparticles decorated reduced graphene oxide for high performance disposable nonenzymatic glucose sensor. Journal of Electroanalytical Chemistry, 743, 1-9.

[14] Gilje, S., Han, S., Wang, M., Wang, K. L., & Kaner, R. B. (2007). A chemical route to graphene for device applications. Nano letters, 7(11), 3394-3398.

[15] Bunch, J.S., Van Der Zande, A.M., Verbridge, S.S., Frank, I.W., Tanenbaum, D.M., Parpia, J.M., Craighead, H.G. and McEuen, P.L. (2007). Electromechanical resonators from graphene sheets. Science, 315(5811), 490-493.

[16] Shan, C., Yang, H., Song, J., Han, D., Ivaska, A., & Niu, L. (2009). Direct electrochemistry of glucose oxidase and biosensing for glucose based on graphene. Analytical Chemistry, 81(6), 2378-2382.

[17] He, Q., Sudibya, H. G., Yin, Z., Wu, S., Li, H., Boey, F., ... & Zhang, H. (2010). Centimeter-long and large-scale micropatterns of reduced graphene oxide films: fabrication and sensing applications. Acs Nano, 4(6), 3201-3208.

[18] Taur, Y., & Ning, T. H. (2013). Fundamentals of modern VLSI devices. Cambridge university press.

[19] Cui, Z., Yin, H., & Nie, Q. (2015). Controllable preparation of hierarchically core–shell structure NiO/C microspheres for non-enzymatic glucose sensor. Journal of Alloys and Compounds, 632, 402-407.

[20] Sun, K. G., & Hur, S. H. (2015). Highly sensitive non-enzymatic glucose sensor based on Pt nanoparticle decorated graphene oxide hydrogel. Sensors and Actuators B: Chemical, 210, 618-623.

[21] Mott, D., Galkowski, J., Wang, L., Luo, J., & Zhong, C. J. (2007). Synthesis of size-controlled and shaped copper nanoparticles. Langmuir, 23(10), 5740-5745.

[22] Eastman, J. A., Choi, S. U. S., Li, S., Yu, W., & Thompson, L. J. (2001). Anomalously increased effective thermal conductivities of ethylene glycol-

based nanofluids containing copper nanoparticles. Applied physics letters, 78(6), 718-720.

[23] Song, J. Y., & Kim, B. S. (2009). Rapid biological synthesis of silver nanoparticles using plant leaf extracts. Bioprocess and biosystems engineering, 32(1), 79-84.

[24] Luo, X., Morrin, A., Killard, A. J., & Smyth, M. R. (2006). Application of nanoparticles in electrochemical sensors and biosensors. Electroanalysis, 18(4), 319-326.

[25] Dang, T. M. D., Le, T. T. T., Fribourg-Blanc, E., & Dang, M. C. (2011). Synthesis and optical properties of copper nanoparticles prepared by a chemical reduction method. Advances in Natural Sciences: Nanoscience and Nanotechnology, 2(1), 015009.

[26] Ayesh, A. I., Karam, Z., Awwad, F., & Meetani, M. A. (2015). Conductometric graphene sensors decorated with nanoclusters for selective detection of Hg 2+ traces in water. Sensors and Actuators B: Chemical, 221, 201-206.

[27] Sharma, V. K., Yngard, R. A., & Lin, Y. (2009). Silver nanoparticles: green synthesis and their antimicrobial activities. Advances in colloid and interface science, 145(1), 83-96.

[28] Ayesh, A. I., Qamhieh, N., Ghamlouche, H., Thaker, S., & El-Shaer, M. (2010). Fabrication of size-selected Pd nanoclusters using a magnetron plasma sputtering source. Journal of Applied Physics, 107(3), 034317.

[29] Al Dosari, H. M., & Ayesh, A. I. (2013). Nanocluster production for solar cell applications. Journal of Applied Physics, 114(5), 054305.

[30] Ayesh, A. I., Qamhieh, N., Mahmoud, S. T., & Alawadhi, H. (2012). Fabrication of size-selected bimetallic nanoclusters using magnetron sputtering. Journal of Materials Research, 27(18), 2441-2446.

[31] Shen, Z., Gao, W., Li, P., Wang, X., Zheng, Q., Wu, H., ... & Ding, K. (2016). Highly sensitive nonenzymatic glucose sensor based on Nickel nanoparticle–attapulgite-reduced graphene oxide-modified glassy carbon electrode. Talanta.

[32] Luo, J., Jiang, S., Zhang, H., Jiang, J., & Liu, X. "A novel non-enzymatic glucose sensor based on Cu nanoparticle modified graphene sheets electrode." Analytica chimica acta709 (2012): 47-53.

[33] Tabrizi, M. A., & Varkani, J. N. (2014). Green synthesis of reduced graphene oxide decorated with gold nanoparticles and its glucose sensing application.Sensors and Actuators B: Chemical, 202, 475-482.

[34] Lu, L. M., Li, H. B., Qu, F., Zhang, X. B., Shen, G. L., & Yu, R. Q. (2011). In situ synthesis of palladium nanoparticle–graphene nanohybrids and their application in nonenzymatic glucose biosensors. Biosensors and Bioelectronics, 26(8), 3500-3504.

[35] Yuan, M., Liu, A., Zhao, M., Dong, W., Zhao, T., Wang, J., & Tang, W. (2014). Bimetallic PdCu nanoparticle decorated three-dimensional graphene hydrogel for non-enzymatic amperometric glucose sensor. Sensors and Actuators B: Chemical, 190, 707-714.

[36] Karuppiah, C., Palanisamy, S., Chen, S. M., Veeramani, V., & Periakaruppan, P. (2014). A novel enzymatic glucose biosensor and sensitive non-enzymatic hydrogen peroxide sensor based on graphene and cobalt oxide nanoparticles composite modified glassy carbon electrode. Sensors and Actuators B: Chemical, 196, 450-456.

[37] Yang, S., Liu, L., Wang, G., Li, G., Deng, D., & Qu, L. (2015). One-pot synthesis of Mn 3 O 4 nanoparticles decorated with nitrogen-doped reduced graphene oxide for sensitive nonenzymatic glucose sensing. Journal of Electroanalytical Chemistry, 755, 15-21.

[38] Xiao, F., Li, Y., Gao, H., Ge, S., & Duan, H. (2013). Growth of coral-like PtAu–MnO 2 binary nanocomposites on free-standing graphene paper for flexible nonenzymatic glucose sensors. Biosensors and Bioelectronics, 41, 417-423.

[39] El Khatib, K. M., & Hameed, R. A. (2011). Development of Cu 2 O/Carbon Vulcan XC-72 as non-enzymatic sensor for glucose determination. Biosensors and Bioelectronics, 26(8), 3542-3548.

[40] Yang, J., Cho, M., Pang, C., & Lee, Y. (2015). Highly sensitive non-enzymatic glucose sensor based on over-oxidized polypyrrole nanowires modified with Ni (OH)2 nanoflakes. Sensors and Actuators B: Chemical, 211, 93-101.

[41] Liu, H., Wu, X., Yang, B., Li, Z., Lei, L., & Zhang, X. (2015). Three-dimensional porous NiO nanosheets vertically grown on graphite disks for enhanced performance non-enzymatic glucose sensor. Electrochimica Acta, 174, 745-752.

[42] Aoun, S. B., Dursun, Z., Koga, T., Bang, G. S., Sotomura, T., & Taniguchi, I. (2004). Effect of metal ad-layers on Au (111) electrodes on electrocatalytic

oxidation of glucose in an alkaline solution. Journal of Electroanalytical Chemistry, 567(2), 175-183.

[43] Cui, H. F., Ye, J. S., Liu, X., Zhang, W. D., & Sheu, F. S. (2006). Pt–Pb alloy nanoparticle/carbon nanotube nanocomposite: a strong electrocatalyst for glucose oxidation. Nanotechnology, 17(9), 2334.

[44] Ayesh, A. I. (2011). Electronic transport in Pd nanocluster devices. Applied Physics Letters, 98(13), 133108.

[45] Ayesh, A. I., Mahmoud, S. T., Ahmad, S. J., & Haik, Y. (2014). Novel hydrogen gas sensor based on Pd and SnO 2 nanoclusters. Materials Letters, 128, 354-357.

[46] Hummers Jr, W. S., & Offeman, R. E., Preparation of graphitic oxide., Journal of the American Chemical Society 80 (6) (1958): 1339-1339.

[47] Paulchamy, B., Arthi, G., & Lignesh, B. D. (2015). A simple approach to stepwise synthesis of graphene oxide nanomaterial. Journal of Nanomedicine & Nanotechnology, 6(1), 1.

[48] Ayesh, A. I. (2016). Linear hydrogen gas sensors based on bimetallic nanoclusters. Journal of Alloys and Compounds, 689, 1-5.

[49] Ayesh, A. I., Ahmed, H. A., Awwad, F., Abu-Eishah, S. I., & Mahmood, S. T. (2013). Mechanisms of Ti nanocluster formation by inert gas condensation. Journal of Materials Research, 28(18), 2622-2628.

[50] Guo, D. J., & Li, H. L. (2005). Highly dispersed Ag nanoparticles on functional MWNT surfaces for methanol oxidation in alkaline solution. Carbon, 43(6), 1259-1264.

[51] Wu, S. H., & Chen, D. H. (2004). Synthesis of high-concentration Cu nanoparticles in aqueous CTAB solutions. Journal of Colloid and Interface Science, 273(1), 165-169.

[52] Song, J. Y., & Kim, B. S. "Rapid biological synthesis of silver nanoparticles using plant leaf extracts." Bioprocess and biosystems engineering 32.1 (2009): 79-84.

[53] Yang, T., Xu, J., Lu, L., Zhu, X., Gao, Y., Xing, H., Yu, Y., Ding, W. and Liu, Z., Copper nanoparticle/graphene oxide/single wall carbon nanotube hybrid materials as electrochemical sensing platform for nonenzymatic glucose detection., Journal of Electroanalytical Chemistry 761 (2016): 118-124.

List of Publications

Said, K., Ayesh, A. I., Qamhieh, N. N., Awwad, F., Mahmoud, S. T., & Hisaindee, S. (2017). *Fabrication and characterization of graphite oxide–nanoparticle composite based field effect transistors for non-enzymatic glucose sensor applications*. Journal of Alloys and Compounds, 694, 1061-1066.